Sandwich-structured photothermal wood for durable moisture harvesting and pumping

Yu-Tang Li, Honglei Chen, Ran Deng, Ming-Bang Wu, Hao-Cheng Yang and Seth B. Darling**

KEYWORDS: Moisture capture, sandwich structure, photothermal, wood, desiccant, dehumidification

ABSRACT: Moisture capture coupled with photothermal regeneration provides an alternative and sustainable way to acquire fresh water. Composite moisture absorbents based on hygroscopic salts are high-efficiency, environmental-friendly and economically feasible, but suffer from the unavoidable desiccant leakage during absorption, and evaporation-induced salt accumulation on material surfaces during desorption. In the current, we develop a superhydrophobic-hydrophilic-hydrophobic photothermal wood embedded with $CaCl_2$ to promote the durability of the absorbents. The sandwich structure serves as a liquid/vapor gate allowing vapor transport but forbidding liquid permeation, enabling the condensation and evaporation within the wood. Beyond moisture harvesting, the sandwich-structured photothermal wood exhibits potential in indoor dehumidification by pumping the moisture through an absorption-desorption cycle.

INTRODUCTION

Worldwide, scientists are seeking alternative access to clean water to tackle looming global water crises originating from climate change, rapid urbanization, and ever-increasing demand. Moisture harvesting is an emerging and attractive way to acquire freshwater since the atmosphere contains an unlimited, replenished source in the form of vapor and small droplets.[1–3] Water production cycles of moisture harvesting normally involve water absorption from humid air by hygroscopic materials and thermal desorption followed by condensing the released vapor into liquid water.

Solar energy provides a sustainable choice of energy source to drive water release at the desorption stage through light-to-heat conversion using photothermal materials. Therefore, solar-driven atmospheric water generators have received immense research interest to realize sustainable water collection by integrating desiccants with photothermal materials.[4] Moisture absorbents play a crucial role in these devices. Liquid desiccants like hygroscopic salt solutions[5], ionic liquids[6] and polyols[7] have been directly applied to absorb moisture and then regenerated by a floating interfacial photothermal evaporator. Although such devices are easy to construct and possess high water-production capacity, they normally require a much larger open liquid area for water sorption than the evaporation area, which lowers the space efficiency and restricts their practical application. Solid porous desiccants, such as zeolites and metal-organic frameworks (MOFs),[8–13] are another category of absorbents that can capture moisture at relatively low humidity. For example, Yaghi's group synthesized a series of Zr- and Al-based MOFs to capture moisture from the air and release water under sunlight, which exhibited impressive water production under relatively low humidity (e.g. 20% RH).[8–10] However, their water absorption capacity is limited by their micro-porous feature, restricting overall water production. Solid hygroscopic salts such as LiCl and $CaCl_2$ are the most common desiccants with high water absorption and low cost, but these materials suffer from similar challenges to the liquid desiccants. The solid salt becomes a liquid solution once absorbing water, which may

cause undesired liquid leakage and salt loss. To mitigate this challenge, hygroscopic salts have been embedded within a porous material or encapsulated within a hydrogel to reserve the liquid.[14–21] For example, Wang's group embedded hygroscopic salts within hollow carbon spheres,[17] silica fibrous filter[15], and polyacrylamide hydrogel[16] to prepare the water-reserving composite absorbents. Entezar *et al*. encapsulated LiCl and $CaCl_2$ within calcium alginate hydrogel for efficient water harvesting.[18] Another strategy to embed hygroscopic salts is to confine hygroscopic salts within the micropores of MOFs[14] or integrate them with MOFs[19] for enhanced water absorption capacity. Although the porous structure or hydrogel can protect the liquid against undesired leakage through capillary effects to a certain extent, salt loss cannot be avoided once the equilibrium adsorption exceeds the maximum water capacity. Moreover, nearly all the hygroscopic-salt-embedded materials face the problem of "salt creep". During the desorption stage, evaporation takes place at the surface and drives the ions to migrate to the surface along with water, leading to salt accumulation at the material surface.[22] Some groups developed hygroscopic-salt-free sorbents such as hydrogels[23,24] to avoid the above issues, but the complicated synthesis process or high cost limits their practical applications.

The most direct solution to salt creep is to prevent the migration of ions from the inner pores to the outer surface. For example, the ions may be rejected by a dense film or gel, but such a physical barrier also increases the diffusion resistance of water molecules, compromising the sorption and desorption performance. To address this issue, here we develop a sandwich-structured wood to seal hygroscopic salt with a wettability gate. The superhydrophobic-hydrophilic-hydrophobic structure can be facilely fabricated by spray-coating polydimethylsiloxane (PDMS) and depositing candle soot on the surface, which allows for vapor diffusion but forbids liquid water flow into or out of the pores.[25] Wood is an ideal reservoir to load hygroscopic salt because the large, rigid, and straight-through porous structure of cellulose and lignin can 1) reserve water within the pores, 2) facilitate vapor diffusion, and 3) resist pore collapse caused by the capillary force during evaporation.[26] The alternate

deposition of PDMS and candle soot endows the surface with both superhydrophobicity and photothermal property. The superhydrophobic surface can protect the wood from contaminants through the self-cleaning effect without hygroscopic salt loss. The sandwich-structured photothermal wood exhibits good moisture capture capacity, which can be adjusted by the types and amount of hygroscopic salts, as well as competitive desorption rate. Moreover, liquid leakage during the absorption stage is prevented by the hydrophobic gate, and the wood also resists salt creep by keeping the evaporation interfaces within the pores. This wood-based device offers potential in solar-enabled dehumidification cycles, which may find use in the adjustment of indoor humidity.

RESULTS AND DISCUSSION

Fabrication and properties of sandwich-structured photothermal wood

The fabrication process of sandwich-structured photothermal wood is presented in Scheme 1. Balsa wood with customized thickness was used to prepare the sandwich-structured device. The edges were sealed with epoxy resin to avoid salt leakage from the side pores. Then, the wood was immersed in $CaCl_2$ solution and dried to load the hygroscopic salts. Both top and bottom surfaces were coated with a thin layer of PDMS by a spray gun for hydrophobic modification. Subsequently, the top surface was suspended on a burning candle to deposit soot, endowing the surface with both photothermal property and superhydrophobicity.[27] PDMS and soot were alternately deposited onto the wood surface several times to stabilize the soot layer. The surface morphology of wood before and after modification was observed by SEM, as shown in Figure 1. The surface pores of bare wood are several tens of micrometers to nearly one hundred micrometers with a porosity of around 82% (**Figure S1**). No significant change in surface morphology can be observed after spray-coating. The thickness of each PDMS coating is 26.7 ± 3.4 nm, as revealed by ellipsometry. Combining with the FTIR spectra, we can conclude a thin and conformal PDMS coating forms on the wood surface (Figure S2). Figure 1i shows the

surface morphology after five deposition cycles of PDMS/candle soot. Some nanostructured features composed of carbon nanoparticles can be observed growing on the wood surface.[28] The hierarchical structure contributes significantly to the superhydrophobicity, and the surface pores are not blocked after PDMS coating and soot deposition. From the SEM images of the cross-section, we can observe $CaCl_2$ particles attaching onto the pore walls. Energy dispersive spectroscopy (EDS) reveals the elemental distribution over the cross-section. As shown in Figure 1b, silicone is concentrated on the top surface of the wood, indicating the permeation of PDMS with a depth of 100~200 μm. On the other hand, calcium is uniformly distributed along the cross-section of the wood below the PDMS-modified layer.

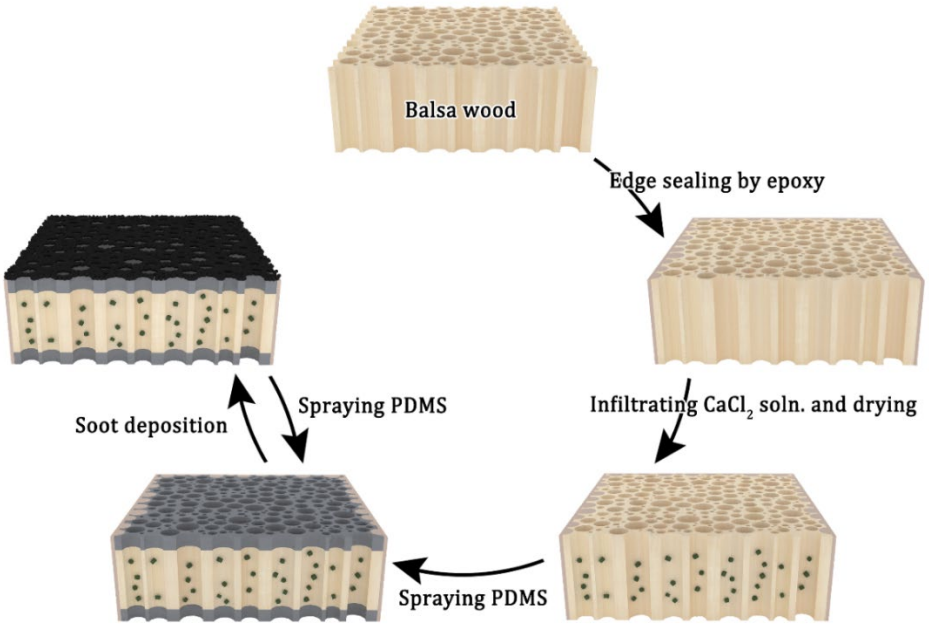

Scheme 1. Fabrication process of sandwich-structured photothermal wood.

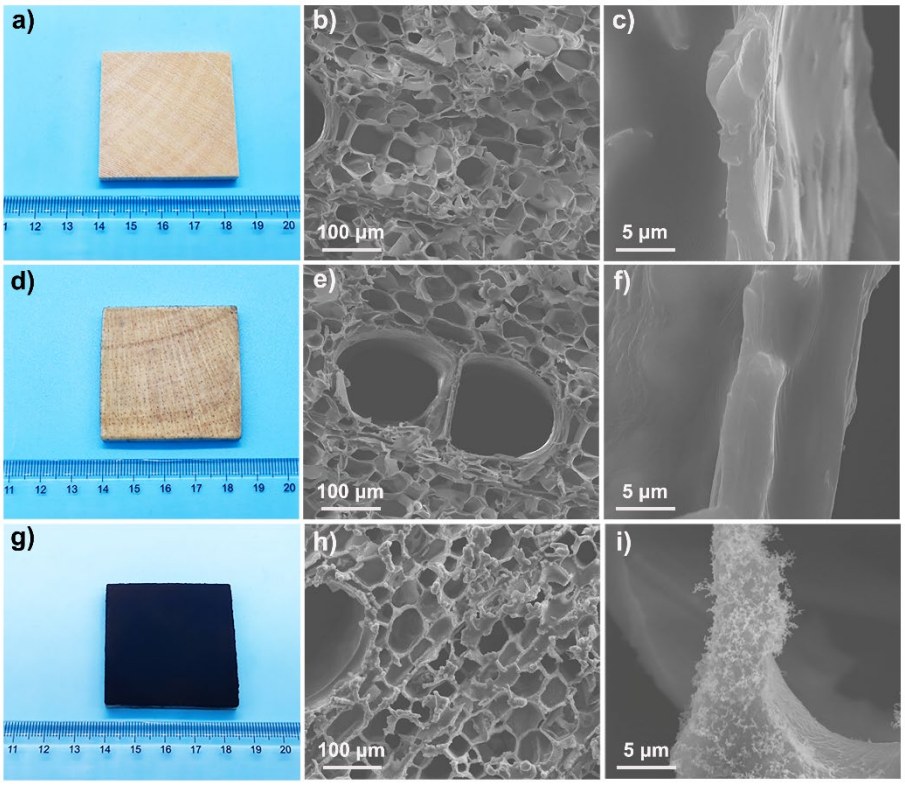

Figure 1. Digital pictures and SEM images of wood surfaces. a-c) Bare wood, d-f) PDMS-coated wood and g-i) candle-soot-deposited wood.

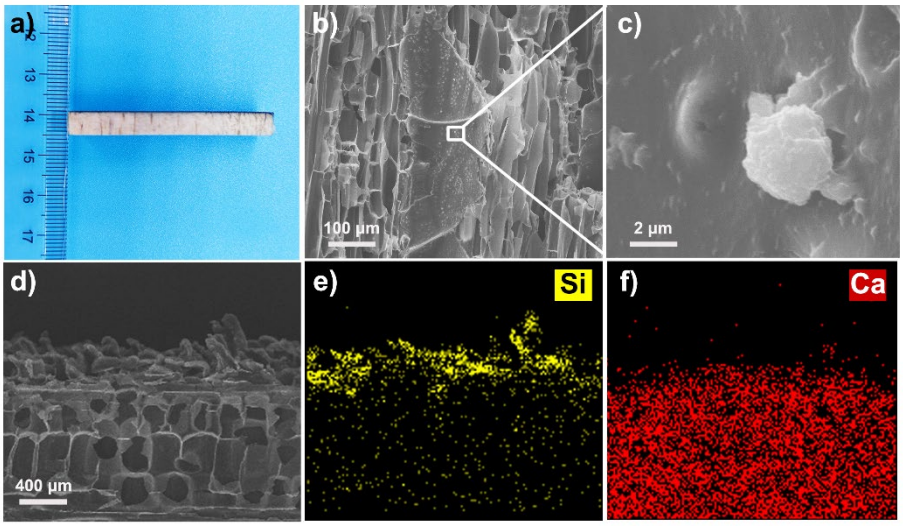

Figure 2. a) Digital pictures and b, c) SEM images of the sandwich-structured wood cross-section. d-f) Elemental distribution on the cross-section of the wood.

The surface wettability is evaluated by the water contact angle (WCA) test. A water droplet (4 µL) gradually penetrates into the bare wood within 1 min as shown in Figure 3a. Both cellulose and lignin contribute to the hydrophilicity of the pores to absorb and reserve water, and similar to other hydrophilic macro-porous materials, the water will permeate through the

wood and shed from the bottom of the material once the pores are fully occupied (Figure S3). After modification by the PDMS, the surface becomes hydrophobic with a WCA around 142°, and the water droplet stands on the surface without permeation. The interface further becomes superhydrophobic with a WCA above 160° after candle soot deposition, as reported in previous studies.[29] PDMS serves as a bonding layer to stabilize the soot layer from peeling. As we mentioned above, the hierarchical structure of the soot layer endows the surface with superhydrophobicity and excellent self-cleaning property. Moreover, different from some Janus structures performing directional water permeation from the hydrophobic side to the hydrophilic side,[30] the hydrophobic layer in this device is thick enough to forbid water permeation from the outside to the inner pores. Therefore, the wood surface is easy to clean by water washing once it is dirtied, without the loss of hygroscopic salt.

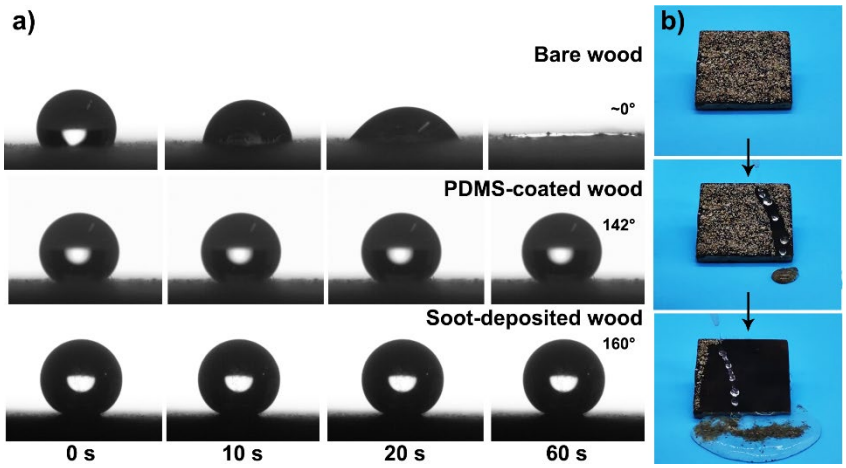

Figure 3. a) Water contact angles on the bare wood, PDMS-coated wood, and soot-deposited wood. b) Demonstrative experiment on the self-cleaning of dirtied sandwich-structured wood.

Moisture capture-and-release performance

The water absorption capacity and rate are crucial parameters for moisture harvesting. We further evaluated the moisture-harvesting performance of the wood. We embedded $CaCl_2$ within the wood by immersing the wood in $CaCl_2$ solution followed by drying. Therefore, the loading amount of $CaCl_2$ can be adjusted by the initial concentration of $CaCl_2$ solution. We measured the mass changes of the wood with a thickness of 5 mm after $CaCl_2$ loading and water

adsorption for 16 h. The projected area of the top surface is a square of 45 mm × 45 mm. As shown in Figure 4a, the $CaCl_2$ loading amount is 0.148 ± 0.014 kg/m^2 with a $CaCl_2$ concentration of 0.1 g/mL, and it gradually increases to 0.412 ± 0.001 kg/m^2 when the $CaCl_2$ concentration increases to 0.5 g/mL. The loaded $CaCl_2$ originates from two sources in principle: the Ca^{2+} adsorbed by the cellulose and lignin in the wood through coordination and the $CaCl_2$ in the solution absorbed within the pores.[31] We measured the two sources of $CaCl_2$ by weighing the pristine wood, $CaCl_2$-embedded wood, and $CaCl_2$-embedded wood rinsed by ultra-pure water until a constant conductivity of the rinse solution, and found the second sources of $CaCl_2$ is more than 99 wt% of the total $CaCl_2$ so that the contribution of water absorption from the first source is negligible.

Water absorption increases with the $CaCl_2$ amount, as expected. We detected the water uptake of the wood at 25 °C and 60% RH for 16 h. The absorption time was determined by two factors. Firstly, the water uptake approaches saturation under the testing temperature and humidity; secondly, the absorption time is normally less than 16 h during a diurnal capture-release cycle of atmospheric water harvesting. The water uptake reaches 0.790 ± 0.033 kg/m^2 for the wood immersed in the $CaCl_2$ solution with a concentration of 0.5 g/mL. We also monitored the water uptake of the wood under 60% RH with time (Figure 4b). The maximum water uptake can be achieved after 8 h with substantial progress within the first 4 h (Figure S4). Water uptake reaches 87.1% of the maximum value after 4 h for the wood immersed in 0.5 g/mL $CaCl_2$ solution and 93.9% for the wood immersed in 0.1 g/mL $CaCl_2$ solution. The rapid initial absorption rate is attributed to the large pores of wood facilitating diffusion of water molecules and high pore-wall area providing more adsorption sites.

According to these results, we selected the 0.5 g/mL $CaCl_2$ solution to load the $CaCl_2$ into the wood in the following experiments. As reported in previous studies, the absorption rate and capacity are also affected by the environment humidity.[16] We recorded the water uptake of the wood at the same temperature (25 °C) but under different humidity (40–80%). The water uptake

of the wood sharply increases to 1.51 ± 0.10 kg/m^2 under 80% RH, nearly double the water uptake of the same wood under 60% RH. The results demonstrate the wood exhibits higher water capture capacity under higher humidity. The water uptake can be also improved by increasing the thickness of the wood. As shown in Figure 4d, the water uptake increases with the wood thickness because of more $CaCl_2$ embedded within the wood as well as increased surface area. It is worth noting that the absorption rate per unit mass of $CaCl_2$ decreases with the thickness because of the growing diffusion resistance with the depth.

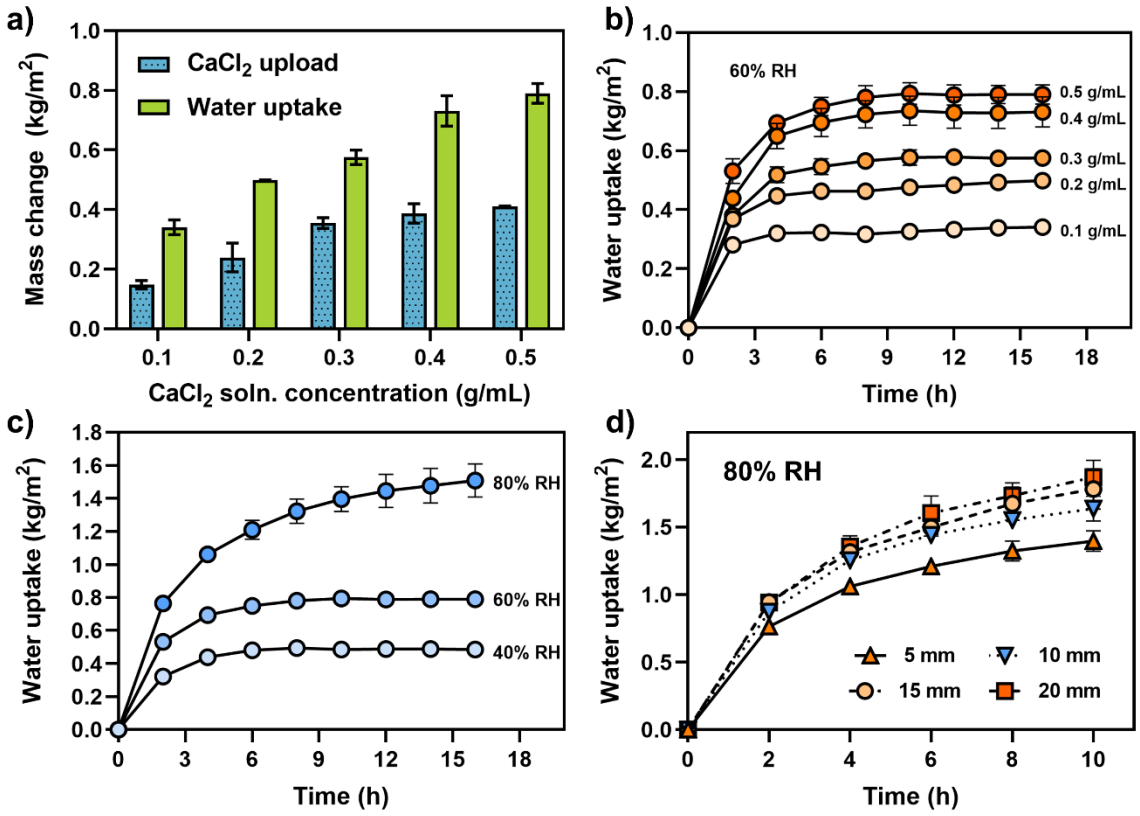

Figure 4. a) Mass changes after loading $CaCl_2$ and absorbing water (16 h) for different sandwich-structured wood. b) Water absorption of sandwich-structured wood immersed in $CaCl_2$ solution with different concentrations. c) Water absorption of sandwich-structured wood under different relative humidity. The $CaCl_2$ solution concentration is 0.5 g/mL, and the wood thickness in a-c is 5 mm. d) Water absorption of sandwich-structured wood with different thicknesses under 80% RH. The $CaCl_2$ solution concentration is 0.5 g/mL.

The light-to-heat conversion efficiency is important for the photothermal desorption process. The UV-Vis-NIR spectra of both bare and sandwich-structured wood were measured to reveal their light absorption properties. As mentioned above, the soot layer acts as the photothermal layer in the sandwich-structured wood, which can absorb nearly 97% of the incident light within

the wavelength range of 200-2100 nm, covering the key segments of the spectrum of sunlight. In contrast, the absorption of the bare balsa wood is relatively weak in the visible and near-infrared regions. The rough surface and aligned large pores contribute to the high light absorption as reported in previous literature[32,33]. We further recorded the temperature evolution on the wood surface under one-sun irradiation by an infrared camera. In the dry state, the surface temperature of sandwich-photothermal wood increases rapidly from room temperature to 73.3 °C within 3 min (Figure S5). After absorbing water, the temperature increases slowly with time because most of the solar energy is converted to latent heat for evaporation. The temperature curve includes two stages. The temperature rapidly rises from room temperature (26.7 °C) to 51.1 °C within 5 min at the initial stage. Then, the temperature is elevated gradually and reaches 68.0 °C after 60 min (Figure 5c). The temperature evolution on our wood for moisture capture is different from that observed with photothermal evaporators for desalination. Instead of reaching a steady balance temperature, the wood presents a slow but continuous temperature rise because of the water loss by evaporation. The simulated sunlight can also induce temperature increase on the bare balsa wood, but the surface temperature is nearly 20 °C lower than that on the sandwich-structured wood.

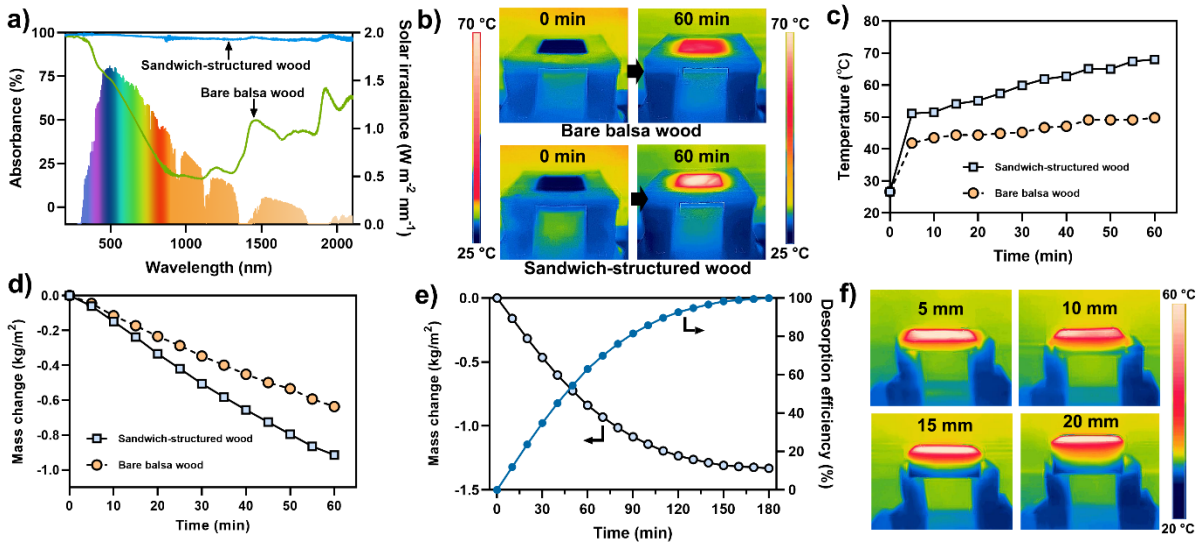

Figure 5. a) UV-Vis-NIR spectra of bare wood and sandwich-structured wood; b) Infrared images of the wood samples under one sun irradiation. c) Evolution of surface temperature on the bare and sandwich-structured wood under simulated sunlight. d) Comparison of mass

changes in different wood samples under simulated sunlight in 1 h. e) Mass change and desorption efficiency of the sandwich-structured wood over 3 h. f) Temperature distribution on the cross-sections of photothermal wood with different thicknesses.

We also compared the evaporation performance of these wood samples (Figure 5d). Under one-sun irradiation, the evaporation rate of sandwich-structured wood reaches 0.90 ± 0.01 $kg \cdot m^{-2} \cdot h^{-1}$, which is much higher than that of the bare wood (0.61 ± 0.03 $kg \cdot m^{-2} \cdot h^{-1}$). The evaporation rate, as well as the photothermal efficiency of the wood, is not competitive to typical reported photothermal evaporators[34] for the following reasons: 1) the evaporation interfaces are in the pores rather than on the wood surface, leading to reduced evaporation area; 2) the heat transfer through the wood is relatively slow, and the water supply is a limiting factor; 3) the relatively high surface temperature leads to reduced photothermal efficiency by increased heat loss. Moreover, the evaporation rate increases at the beginning and then decrease significantly with time, in particular after 2 h, as shown in Figure 5e. The increase in the evaporation rate corresponds to the temperature rise at the initial stage, and the decrease is attributed to the elevated vaporization enthalpy of the concentrated $CaCl_2$ solution.[5] On the other hand, nearly 60% of the absorbed water evaporates after 1 h irradiation, indicating the desorption process is more efficient than the absorption process. Considering the dramatically increased evaporation heat of the concentrated solution in the wood, the desorption efficiency in practical application could be below 100%. In addition, although there is a slight decrease in desorption rate for the wood samples with different thicknesses, the decrease is not significant, so the moisture-harvesting capacity can be promoted by using thicker wood (Figure S6). The evaporation performance reduction with increased wood thickness is caused by poor heat conduction (Figure 5f and S7). The thermal conductivity of dried and wet wood samples is 0.095 ± 0.025 W/m·K and 0.200 ± 0.052 W/m·K respectively, and increasing the thermal conductivity of the wood will promote the practicability of thick wood materials in future research.

Wettability gating preventing liquid leakage and salt creep

In the sandwich-structured wood, the hydrophobic layer acts as a gate allowing vapor transport while preventing liquid water permeation (Scheme 2). This design can preserve the absorbed water from undesired leakage. We compared the water absorption behavior of the bare balsa wood and sandwich-structured wood infiltrated with the same amount of $CaCl_2$. The wood samples were placed on an evaporating dish at 80% RH for 12 h. As displayed in Figure 6a and b, some liquid was left in the evaporating dish for the bare balsa wood whereas no water leakage was observed for the sandwich-structured wood. The mass change of the sandwich-structured wood (Figure 6c and d) is slightly lower than the mass change of bare balsa wood system (the weight gain for the sandwich-structured sample reaches nearly 95% of that on the bare one) because the unconfined water outside the material can freely absorb the moisture without any diffusion resistance. However, the water uptake in the sandwich-structured wood is higher than that of the bare balsa wood after removing the unconfined water. In addition, nearly 16.4% of absorbed water leaks out from the bare wood, which means the same percentage of $CaCl_2$ may be lost during an absorption-desorption cycle if the $CaCl_2$ concentration in the wood is uniform. In a reusability test, the sandwich-structured wood was placed in a humidity chamber to absorb water at 25 °C and 80% RH for 10 h, and to desorb water in an oven at 60 °C. Although the water uptake fluctuates somewhat between the adsorption-desorption cycles, the device retains 92% of the maximum water uptake after 10 cycles (Figure 6e). In contrast, the $CaCl_2$-embedded wood without hydrophobic layers shows a sharp reduction of water absorption capacity in the first cycle, and the capacity gradually decreases to less than 80% of the initial water uptake after 10 cycles (Figure S8).

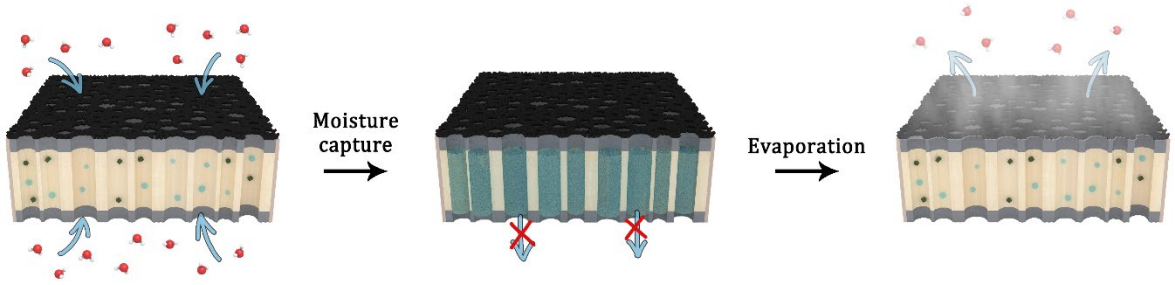

Scheme 2. Working principles of sandwich-structured photothermal wood.

Another challenge of conventional hygroscopic-salt-loaded materials is salt creep during evaporation. Since the evaporation takes place at the air-liquid interface, the directional water flow caused by evaporation brings the solute to the surface, leading to scaling on the surface once the surface is desiccated. As a result, the hygroscopic salt embedded within the pores will be gradually transferred to the outer surface. Salt creep not only affects the subsequent evaporation process by covering the photothermal surface, but also exacerbates the problem of salt loss. We fabricated a surface-carbonized balsa wood sample as a control, which has a hydrophilic surface and allows for water permeation (Figure S9). Both carbonized wood and sandwich-structured wood loaded with same amount of $CaCl_2$ were placed in the humidity chamber at 80% RH for 10 h and then transferred under the simulated sunlight for photothermal desorption. As presented in Figure 6f and g, a white region appeared at the middle of the carbonized wood surface after 10 min, and gradually extended over the surface. In contrast, no significant change was observed on the surface of sandwich-structured wood, because the evaporating interface was below the photothermal surface.

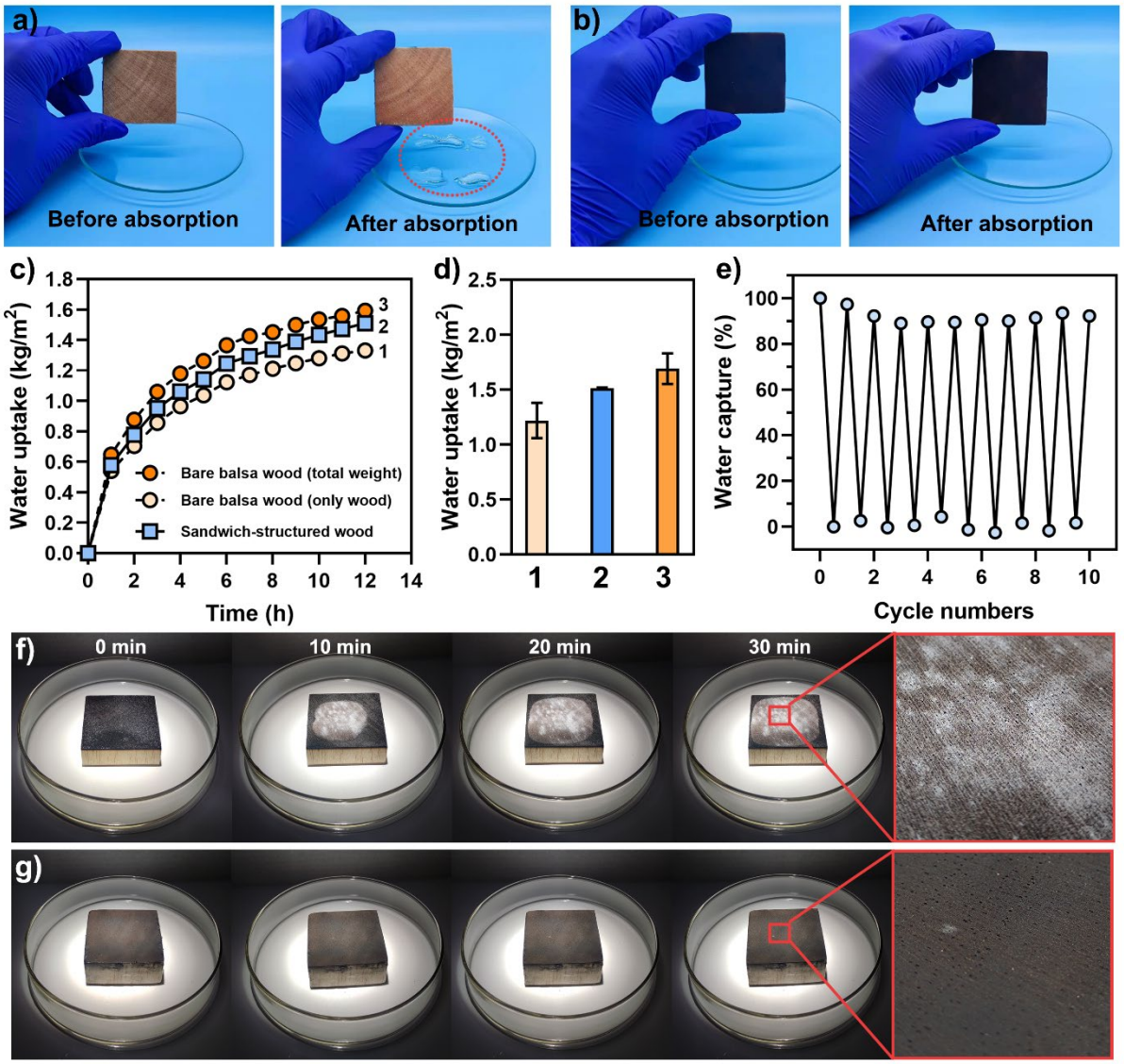

Figure 6. Water absorption in a) bare balsa wood and b) sandwich-structured wood. c) Water uptake changes and d) final water uptake after 12 h absorption on bare balsa wood and sandwich-structured wood. e) Reusability of the sandwich-structured wood. Salt creep tests on the f) carbonized and g) sandwich-structured wood samples.

Conceptual moisture pumping for humidity adjustment

We conducted demonstrative experiments to explore the potential of sandwich-structured wood in moisture harvesting (Figure 7a). Five pieces of wood were placed in a homemade apparatus. The apparatus was placed outdoors and opened to the atmosphere for moisture capture at night (RH 85%-90%, 28-30 °C). Then, we closed the transparent cover and placed the collector under sunlight at daytime (35-41 °C). The sorption time was 12 h, and the absorbed water was released in 3 h at noon. Small water droplets condensed on the inner surface of the cover after 1 h and

coalesced into large droplets over time, and the final water production was 4.34 kg/m^2 (Figure S10). The sandwich-structured photothermal wood can serve as a moisture pump to adjust the indoor moisture. We put a wood sample with a nominal area of 45 mm × 45 mm on the roof of a house model (dimensions are presented in Figure S11) for a moisture-pumping experiment (Figure 7b). The initial humidity in the house model was adjusted to 90% by a humidifier, and the house was placed under a sunlight simulator. As shown in Figure 7c, the indoor humidity gradually decreased from 90% RH to 62 % RH within 1 h, even lower than the outside humidity of around 70% RH. At the same time, the indoor temperature shows negligible increase (from 24.2 °C to 24.4 °C). During this process, the moisture is captured by the wood and then evaporated to the outdoor atmosphere. The vapor mostly escapes from the outside because the higher temperature of the heating surface, although it can in principle transport through both faces of the wood. As mentioned above, the thermal conductivity of the wood is relatively low, so the photothermal heating cannot affect the indoor temperature significantly. Moreover, compared with reported moisture pumps made by nanofibrous membranes,[19] the wood exhibits superior mechanical strength and thermal insulation as a building material.

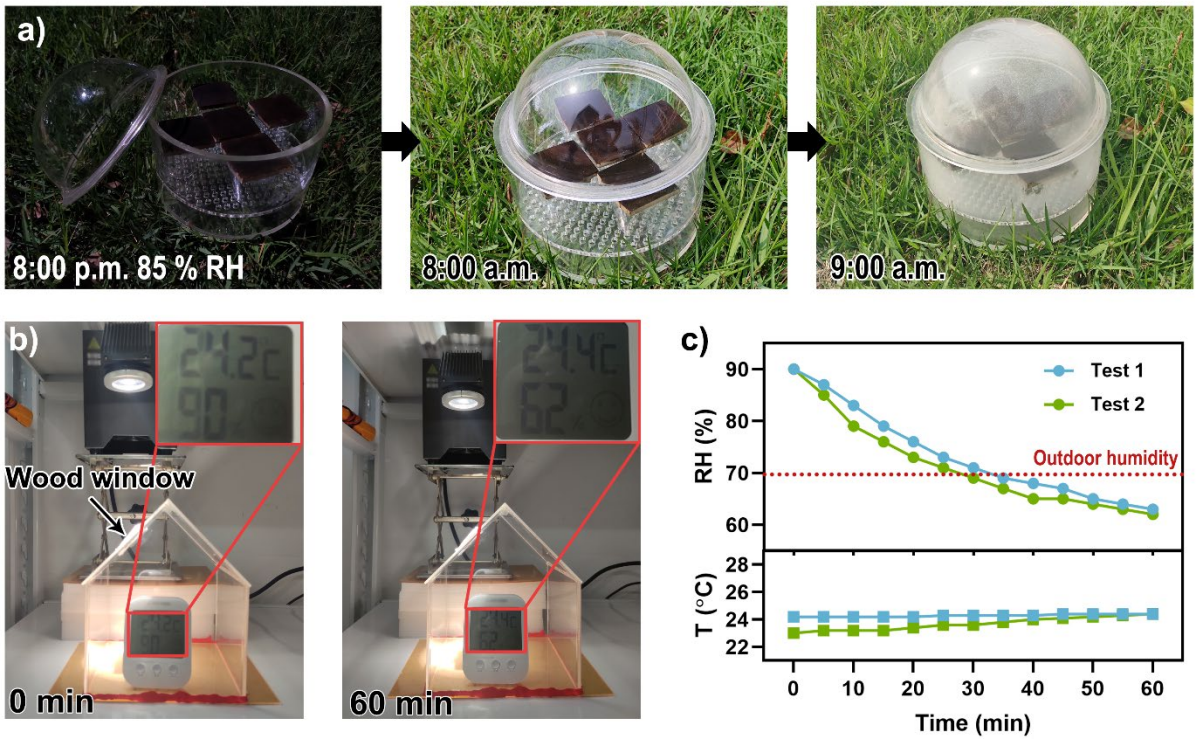

Figure 7. a) Demonstrative experiment of moisture harvesting by a home-made apparatus. b) demonstrative experiment of a house model equipped with the sandwich-structured photothermal wood. c) Humidity and temperature changes in the house model.

CONCLUSION

In summary, we developed a sandwich-structured photothermal wood device for moisture capture from the atmosphere. The hygroscopic salt, $CaCl_2$, was embedded within the wood pores and sealed by hydrophobic gates made of PDMS and candle soot. Such a structure allows for vapor transport during the absorption and desorption stages, but prevents liquid transport out of the wood. By tuning the $CaCl_2$ concentration during fabrication, a maximum absorption capacity of 1.51 ± 0.10 kg/m^2 was achieved for the wood with a thickness of 5 mm at 25 °C and 80% RH. The water absorption capacity might be further promoted by replacing the $CaCl_2$ with other hygroscopic materials. Moreover, the sandwich-structured wood can reserve the liquid within the device during the absorption process, and thereby prevent salt creep at the desorption stage. Therefore, the wood exhibits excellent durability without significant performance compromise. Beyond moisture capture, the sandwich-structured photothermal wood displays potential in indoor dehumidification because it can pump the moisture through an absorption-desorption cycle.

EXPERIMENT SECTION

Materials. Calcium chloride ($CaCl_2$, ≥ 96%) was obtained from Sinopharm Chemical Reagent Co., Ltd, China. PDMS prepolymer (SYLGARD 184A) and thermal curing agent (SYLGARD 184B) were purchased from Dow Corning, U.S.A. Candles and balsa wood (45×45×5 mm) are commercial products. Epoxy resin(E-44) was provided by Guangdong Zhujiang Chemical Coating Co. Ltd. Diethylenetriamine (99%), n-hexane (99%) were supplied by Macklin Biochemical Co., Ltd., China. Deionized (DI) water was produced by an ultra-pure water system (Aquaplore-2s). All chemical agents were utilized without further purification.

Preparation of sandwich-structured wood. A mixture of epoxy resin and diethylenetriamine with a mass ratio of 10:1 was stirred at 25 °C for 15 min, and then defoamed by centrifugation. The side edges of balsa wood were coated with the epoxy resin and cured at room temperature for four hours. The sealed balsa wood was washed in an ultrasonic cleaner for 10 min before $CaCl_2$ infiltration. Subsequently, the clean balsa wood was impregnated in the $CaCl_2$ solutions with a concentration from 0.1 to 0.5 g/mL for 90 min under vacuum and then dried overnight at 60 °C. To fabricate the PDMS coating, pre-polydimethylsiloxane, n-hexane and crosslinking agent were mixed and stirred at 25 °C for 30 min with a mass ratio of 10:10:1 to prepare the coating solution. Then the solution was sprayed onto both surfaces of balsa wood by a spray gun (Airbrush XinJianDa Co. Ltd.). The spraying time is 3 s to avoid surface pore blocking, To deposit the soot, the depositing surface was placed at a height of 2 cm above the flame and moved uniformly[35]. The spray-coating of PDMS and deposition of soot were alternately conducted to achieve a stable superhydrophobic photothermal layer. Surface-carbonized wood was fabricated by pressing the pristine wood on a hot stage at 400 °C for 3 s.

Characterization. The surface and cross-section morphologies of the sandwich-structured wood were investigated using a field-emission scanning electron microscope (Quanta 400F, FEI). The element distribution in the cross-section of sandwich-structured wood was characterized by EDS (Energy dispersive spectrometer). We further analyzed the pore-size distribution and porosity from the SEM image by *Image J*. The reflection spectra in UV-Vis-NIR region was detected by a spectrometer (Lambda950, PerkinElmer). The water contact angles (WCA) were recorded on a water contact angle test system (CA15EC, Dataphysics) with a droplet volume of 4 μL. To estimate the thickness of PDMS coating, we spray-coated the PDMS on a silicon wafer under the same conditions and measured the PDMS thickness by an ellipsometer (RC2, J.A. Woollam). The thermal conductivity of the wood was detected by a quick thermal conductivity meter (XIATECH TC3200).

Moisture absorption and desorption measurements. The moisture absorption capacity and absorption-desorption cycle stability of the samples were evaluated in a constant temperature and humidity chamber (BSP-50CL, YI HENG). The moisture absorption tests were performed at 25 °C within a wide range of humidity (40, 60, 80% RH). The samples were dried in an oven at 60 °C to a constant weight before testing, and then placed at a constant temperature and humidity. Samples were taken out each 2 hours for weighting. During the absorption–desorption cycle, the samples were kept at 25 °C and 80% RH for 10 hours to absorb moisture and transferred to a oven for desorption at 60 °C for 14 hours. The water evaporation test was performed under a standard solar simulator (Sirius-SS150-D, Zolix). The solar radiation intensity was controlled at 1 kW/m^2. The surface temperature of the sample was measured by an infrared camera (one pro, FLIR). The environment temperature is maintained at ~25 °C) and the relative humidity of ~50%.

ASSOCIATED CONTENT

Supporting Information

More detailed experimental data, characterization, and supplementary figures.

Pore size distribution of the wood, ATR-FTIR spectra, demonstrative experiments, temperature evolution, infrared images, water contact angles, cycling test (PDF)

AUTHOR INFORMATION

Corresponding Author

Hao-Cheng Yang – School of Chemical Engineering and Technology, Sun Yat-sen University, Southern Marine Science and Engineering Guangdong Laboratory (Zhuhai), Zhuhai, 519082, China

E-mail: yanghch8@mail.sysu.edu.cn

Seth B. Darling – Center for Molecular Engineering and Chemical Sciences and Engineering Division, Argonne National Laboratory, Lemont, IL 60439, USA

Advanced Materials for Energy-Water Systems (AMEWS) Energy Frontier Research Center, Argonne National Laboratory, Lemont, IL 60439, USA

E-mail: darling@anl.gov

Authors

Yu-Tang Li – School of Chemical Engineering and Technology, Sun Yat-sen University, Southern Marine Science and Engineering Guangdong Laboratory (Zhuhai), Zhuhai, 519082, China

Honglei Chen – School of Chemical Engineering and Technology, Sun Yat-sen University, Southern Marine Science and Engineering Guangdong Laboratory (Zhuhai), Zhuhai, 519082, China

Ran Deng – School of Chemical Engineering and Technology, Sun Yat-sen University, Southern Marine Science and Engineering Guangdong Laboratory (Zhuhai), Zhuhai, 519082, China

Ming-Bang Wu – School of Materials Science and Engineering, Zhejiang Sci-Tech University, Hangzhou 310018, China

Author Contributions

Y.-T. Li performed the experiments, analyzed the data, and prepared the manuscript. H. Chen contributed to the experiments and data analysis. R. Deng and M.-B. Wu contributed to the manuscript preparation. H.-C. Yang and S.B. Darling designed the experiments, wrote and revised the manuscript.

Notes

The authors declare no competing financial interest.

ACKNOWLEDGMENTS

This work was financially supported by the National Natural Science Foundation of China (51909291), the Guangzhou Scientific and Technological Planning Project (202002030181) and Fundamental Research Funds for the Central Universities (19lgzd17). S.B.D. was supported as part of the Advanced Materials for Energy-Water-Systems (AMEWS) Center, an Energy Frontier Research Center funded by the U.S. Department of Energy, Office of Science, Basic Energy Sciences. We also thank Mr. S.-L. Wu for his contributions during the experiments.

REFERENCES

(1) Zhou, X.; Lu, H.; Zhao, F.; Yu, G. Atmospheric Water Harvesting: A Review of Material and Structural Designs. *ACS Mater. Lett.* **2020**, *2*, 671–684.

(2) Vanderschaeghe, H.; Martens, J. A. Energy Performance and Climate Dependency of Technologies for Fresh Water Production from Atmospheric Water Vapour. *Environ. Sci. Water Res. Technol.* **2020**, *6*, 2016–2034.

(3) LaPotin, A.; Kim, H.; Rao, S. R.; Wang, E. N. Adsorption-Based Atmospheric Water Harvesting: Impact of Material and Component Properties on System-Level Performance. *Acc. Chem. Res.* **2019**, *52*, 1588–1597.

(4) Chen, H.; Wu, S.-L.; Wang, H.-L.; Wu, Q.-Y.; Yang, H.-C. Photothermal Devices for Sustainable Uses Beyond Desalination. *Adv. Energy Sustain. Res.* **2021**, 2000056.

(5) Wang, X.; Li, X.; Liu, G.; Li, J.; Hu, X.; Xu, N.; Zhao, W.; Zhu, B.; Zhu, J. An Interfacial Solar Heating Assisted Liquid Sorbent Atmospheric Water Generator. *Angew. Chemie - Int. Ed.* **2019**, *58*, 12054–12058.

(6) Qi, H.; Wei, T.; Zhao, W.; Zhu, B.; Liu, G.; Wang, P.; Lin, Z.; Wang, X.; Li, X.; Zhang, X.; et al. An Interfacial Solar-Driven Atmospheric Water Generator Based on a Liquid Sorbent with Simultaneous Adsorption–Desorption. *Adv. Mater.* **2019**, *31*, 1903378.

(7) Ni, F.; Qiu, N.; Xiao, P.; Zhang, C.; Jian, Y.; Liang, Y.; Xie, W.; Yan, L.; Chen, T. Tillandsia-Inspired Hygroscopic Photothermal Organogels for Efficient Atmospheric Water Harvesting. *Angew. Chemie - Int. Ed.* **2020**, *59*, 19237–19246.

(8) Kim, H.; Rao, S. R.; Kapustin, E. A.; Zhao, L.; Yang, S.; Yaghi, O. M.; Wang, E. N. Adsorption-Based Atmospheric Water Harvesting Device for Arid Climates. *Nat. Commun.* **2018**, *9*, 1191.

(9) Kim, H.; Yang, S.; Rao, S. R.; Narayanan, S.; Kapustin, E. A.; Furukawa, H.; Umans, A. S.; Yaghi, O. M.; Wang, E. N. Water Harvesting from Air with Metal-Organic Frameworks Powered by Natural Sunlight. *Science.* **2017**, *356*, 430–434.

(10) Fathieh, F.; Kalmutzki, M. J.; Kapustin, E. A.; Waller, P. J.; Yang, J.; Yaghi, O. M. Practical Water Production from Desert Air. *Sci. Adv.* **2018**, *4*, eaat3198.

(11) Canivet, J.; Fateeva, A.; Guo, Y.; Coasne, B.; Farrusseng, D. Water Adsorption in MOFs: Fundamentals and Applications. *Chem. Soc. Rev.* **2014**, *43*, 5594–5617.

(12) Kalmutzki, M. J.; Diercks, C. S.; Yaghi, O. M. Metal–Organic Frameworks for Water Harvesting from Air. *Adv. Mater.* **2018**, *30*, 1704304.

(13) Xu, J.; Chao, J.; Li, T.; Yan, T.; Wu, S.; Wu, M.; Zhao, B.; Wang, R. Near-Zero-Energy Smart Battery Thermal Management Enabled by Sorption Energy Harvesting from Air. *ACS Cent. Sci.* **2020**, *6*, 1542–1554.

(14) Xu, J.; Li, T.; Chao, J.; Wu, S.; Yan, T.; Li, W.; Cao, B.; Wang, R. Efficient Solar-Driven Water Harvesting from Arid Air with Metal–Organic Frameworks Modified by Hygroscopic Salt. *Angew. Chemie - Int. Ed.* **2020**, *59*, 5202–5210.

(15) Li, R.; Shi, Y.; Shi, L.; Alsaedi, M.; Wang, P. Harvesting Water from Air: Using Anhydrous Salt with Sunlight. *Environ. Sci. Technol.* **2018**, *52*, 5398–5406.

(16) Li, R.; Shi, Y.; Alsaedi, M.; Wu, M.; Shi, L.; Wang, P. Hybrid Hydrogel with High Water Vapor Harvesting Capacity for Deployable Solar-Driven Atmospheric Water Generator. *Environ. Sci. Technol.* **2018**, *52*, 11367–11377.

(17) Li, R.; Shi, Y.; Wu, M.; Hong, S.; Wang, P. Improving Atmospheric Water Production Yield: Enabling Multiple Water Harvesting Cycles with Nano Sorbent. *Nano Energy* **2020**, *67*, 104255.

(18) Entezari, A.; Ejeian, M.; Wang, R. Super Atmospheric Water Harvesting Hydrogel with Alginate Chains Modified with Binary Salts. *ACS Mater. Lett.* **2020**, *2*, 471–477.

(19) Zhang, Y.; Wu, L.; Wang, X.; Yu, J.; Ding, B. Super Hygroscopic Nanofibrous Membrane-Based Moisture Pump for Solar-Driven Indoor Dehumidification. *Nat. Commun.* **2020**, *11*, 3302.

(20) Wang, M.; Sun, T.; Wan, D.; Dai, M.; Ling, S.; Wang, J.; Liu, Y.; Fang, Y.; Xu, S.; Yeo, J.; et al. Solar-Powered Nanostructured Biopolymer Hygroscopic Aerogels for Atmospheric Water Harvesting. *Nano Energy* **2021**, *80*, 105569.

(21) Yan, T.; Li, T.; Xu, J.; Chao, J.; Wang, R.; Aristov, Y. I.; Gordeeva, L. G.; Dutta, P.; Murthy, S. S. Ultrahigh-Energy-Density Sorption Thermal Battery Enabled by Graphene Aerogel-Based Composite Sorbents for Thermal Energy Harvesting from Air. *ACS Energy Lett.* **2021**, *6*, 1795–1802.

(22) Wu, M.; Li, R.; Shi, Y.; Altunkaya, M.; Aleid, S.; Zhang, C.; Wang, W.; Wang, P. Metal- and Halide-Free, Solid-State Polymeric Water Vapor Sorbents for Efficient Water-Sorption-Driven Cooling and Atmospheric Water Harvesting. *Mater. Horizons* **2021**, *8*, 1518–1527.

(23) Wu, M.; Li, R.; Shi, Y.; Altunkaya, M.; Aleid, S.; Zhang, C.; Wang, W.; Wang, P. Metal- and Halide-Free, Solid-State Polymeric Water Vapor Sorbents for Efficient Water-Sorption-Driven Cooling and Atmospheric Water Harvesting. *Mater. Horizons* **2021**, *8*, 1518–1527.

(24) Nandakumar, D. K.; Zhang, Y.; Ravi, S. K.; Guo, N.; Zhang, C.; Tan, S. C. Solar Energy Triggered Clean Water Harvesting from Humid Air Existing above Sea Surface Enabled by a Hydrogel with Ultrahigh Hygroscopicity. *Adv. Mater.* **2019**, *31*, 1806730.

(25) Luo, Y.-Q.; Song, F.; Xu, C.; Wang, X.-L.; Wang, Y.-Z. Bioinspired Fabrication of Asymmetric Wood Materials for Directional Liquid Manipulation and Transport. *Chem. Eng. J.* **2020**, *383*, 123168.

(26) Yang, H. C.; Chen, Y. F.; Ye, C.; Jin, Y. N.; Li, H.; Xu, Z. K. Polymer Membrane with a Mineral Coating for Enhanced Curling Resistance and Surface Wettability. *Chem. Commun.* **2015**, *51*, 12779–12782.

(27) Peeters, R.; Vanderschaeghe, H.; Rongé, J.; Martens, J. A. Energy Performance and Climate Dependency of Technologies for Fresh Water Production from Atmospheric Water Vapour. *Environ. Sci. Water Res. Technol.* **2020**, *6*, 2016–2034.

(28) Sahoo, B. N.; Kandasubramanian, B. An Experimental Design for the Investigation of Water Repellent Property of Candle Soot Particles. *Mater. Chem. Phys.* **2014**, *148*, 134–142.

(29) Iqbal, R.; Majhy, B.; Sen, A. K. Facile Fabrication and Characterization of a PDMS-Derived Candle Soot Coated Stable Biocompatible Superhydrophobic and Superhemophobic Surface. *ACS Appl. Mater. Interfaces* **2017**, *9*, 31170–31180.

(30) Yang, H. C.; Xie, Y.; Hou, J.; Cheetham, A. K.; Chen, V.; Darling, S. B. Janus Membranes: Creating Asymmetry for Energy Efficiency. *Adv. Mater.* **2018**, *30*, 1801495.

(31) Barbetta, A.; Fratzl, P.; Zemb, T.; Bertinetti, L. Impregnation and Swelling of Wood with Salts: Ion Specific Kinetics and Thermodynamics Effects. *Adv. Mater. Interfaces* **2017**, *4*, 1600437.

(32) Zhu, M.; Li, Y.; Chen, F.; Zhu, X.; Dai, J.; Li, Y.; Yang, Z.; Yan, X.; Song, J.; Wang, Y.; et al. Plasmonic Wood for High-Efficiency Solar Steam Generation. *Adv. Energy Mater.* **2018**, *8*, 1701028.

(33) Li, T.; Liu, H.; Zhao, X.; Chen, G.; Dai, J.; Pastel, G.; Jia, C.; Chen, C.; Hitz, E.; Siddhartha, D.; et al. Scalable and Highly Efficient Mesoporous Wood-Based Solar Steam Generation Device: Localized Heat, Rapid Water Transport. *Adv. Funct. Mater.* **2018**, *28*, 1707134.

(34) Wu, S. L.; Chen, H.; Wang, H. L.; Chen, X.; Yang, H. C.; Darling, S. B. Solar-Driven Evaporators for Water Treatment: Challenges and Opportunities. *Environ. Sci. Water Res. Technol.* **2021**, *7*, 24–39.

(35) Liu, X.; Zhang, X.; Chen, Q.; Pan, Y.; Liu, C.; Shen, C. A Simple Superhydrophobic/Superhydrophilic Janus-Paper with Enhanced Biocompatibility by PDMS and Candle Soot Coating for Actuator. *Chem. Eng. J.* **2021**, *406*, 126532.
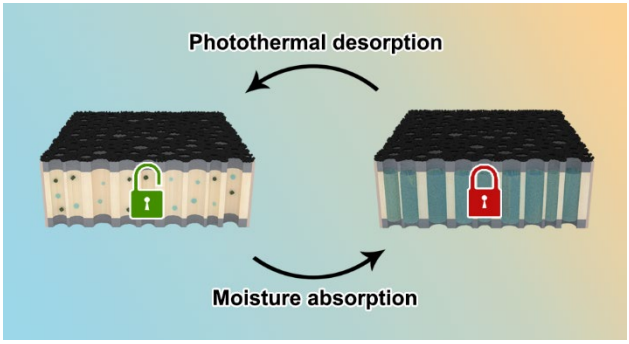
Table of Content